Multi-scale Simulation Study of Pt-Alloys Degradation for Fuel Cells Applications

G. Ramos-Sánchez, Nhi Dang and Perla B. Balbuena

Abstract Low-temperature fuel cells are one of the most promising systems for the transformation of fuels in an efficient, silent, and environmentally friendly manner. The requirements for the electrocatalyst are essentially three: the highest possible catalytic activity and the longest life cycle at the lowest cost. Sometimes, we can obtain one at expenses of the other. In this chapter, we review the simulation methods used in our group to study the degradation of catalysts for fuel cell applications: Density functional theory (DFT), classical molecular dynamics (CMD), Ab initio molecular dynamics (AIMD), and kinetic Monte Carlo (KMC). In the first part, we employ DFT, AIMD, and CMD to address the importance of the oxygen concentration on the surface of the catalysts and its influence on the "buckling" of Pt atoms and the role of the subsurface atoms. Then we analyze the temporal evolution of shape and composition of Pt/Ni nanoalloys by KMC simulations at various overall compositions and applied voltages. Finally, using DFT we study the effect that the presence of oxygen in the subsurface has on the buckling of Pt skin/PtCo structures by varying the oxygen coverage factor. The different methods and time scales used for the simulations permit us to fathom the factors governing the stability of electrocatalysts for fuel cells applications.

1 Introduction

In the last centuries, fossil fuels have helped mankind to obtain increasing levels of comfort and wellness. Unfortunately, the use of fossil fuels has also caused detrimental effects on the environmental global conditions. Now it is widely accepted that the global warming and climate change are caused directly by human activity, specially owed to CO_2 emissions generated by energy and transportation demands.

G. Ramos-Sánchez · N. Dang · P.B. Balbuena (✉)
Department of Chemical Engineering, Texas A&M University, College Station, TX 77843, USA
e-mail: balbuena@tamu.edu

A.A. Franco et al. (eds.), *Physical Multiscale Modeling and Numerical Simulation of Electrochemical Devices for Energy Conversion and Storage*, Green Energy and Technology, DOI 10.1007/978-1-4471-5677-2_2

Despite many actions proposed by international organisms in the reduction of greenhouse gases, and promotion of conscious usage of the automobile, the CO_2 and CO emissions are continuously increasing to values that may lead to unthinkable consequences [1]. Renewable energies are promising alternatives to the use of fossil fuels: solar, wind, and sea are practically infinite and free energy sources if we find a cheap way to convert, storage, and transmit them. Solar energy, wind, and hydropower cannot be widely used without converting into electricity or chemical energy carriers. The favored chemical energy carriers are hydrogen and methanol because of their "easy" generation, respectively, from water and carbon dioxide, both lead to a drastic CO_2 reduction compared to the fossil-based concepts [2]. Low-temperature fuel cells (Polymer electrolyte fuel cells, PEFC) represent an environmentally friendly technology and are attracting considerable interest as a means of producing electricity by direct electrochemical conversion of hydrogen/methanol and oxygen into water and carbon monoxide.

There are, however, severe shortcomings on the present technologies, which need to be overcome to make low-temperature fuel cells economically attractive. One of the most important problems is related to the low rate of the cathodic reaction, the oxygen reduction reaction (ORR). Platinum has been widely used for this reaction, but due to kinetic limitations the cathodic overpotential losses amount to 0.3–0.4 V under typical PEFC operating conditions. Improvements have been made, especially by alloying or modifying the composition of the cathodic nanoparticle. The improvement in the ORR electrocatalysts of Pt-alloys has been ascribed to different structural changes caused by lattice mismatch producing decreased Pt–Pt distances and electronic or ligand effects in which a different environment causes the modification of the density of states responsible of the coupling with the oxygen molecule. Pt/Co and Pt/Ni catalysts in different structural configurations and proportions of its components have been proposed to be among the most active materials able to overcome the large energy barrier for the electrochemical reduction of molecular oxygen [3–7].

Tremendous improvements in power density and cost reduction of polymer electrolyte fuel cells have been achieved over the last two decades, which have brought PEFC systems close to the benchmarks that are critical for commercialization [8]; however, several other problems have arose, and these issues are mostly related to the time evolution of the electrode materials. Electrode durability is now one of the main shortcomings limiting the large-scale development and commercialization of this zero-emission power technology. The change in the microstructure is related to degradation/corrosion of the catalytic layers components: carbon and platinum-based nanoparticles, but also corrosion of other components is possible: membrane degradation and corrosion of the bipolar plates. It is widely reported that the electrochemical and microstructural properties of Pt and Pt-alloy electrodes evolve during the membrane electrode assembly (MEA) operation and in typical three electrode probes [9–11]. Degradation of the membrane has been related to radical attack coming from hydrogen peroxide produced in the two-electron oxygen reduction [12]; this is detrimental because it ultimately results in membrane pin-hole formation, which is the main cause of cell failure. The resultant structure after

catalysts and substrate degradation eventually leads to the formation of cracks and in consequence to the separation of membrane and catalytic layer with final consequences such as increase in total resistance, decrease of cell voltage, increase of mass transport issues, decrease of the initially optimized 3D structures, etc.; all these phenomena drive unacceptable performance losses over time and eventually cell failure [13]. In this work, we focus on the degradation problems originated in the structure and composition of the catalytic material, particularly in the alloyed catalysts where the inclusion of a second or third alloying metal causes different durability properties than those of pure Platinum.

For nanoalloys in spite of the great deal of efforts set on the synthesis, it is very likely that the synthesized compounds appear very promising regarding size distributions, and other desirable features, once in the electrochemical media of fuel cells their structure changes rapidly; so different experimental and theoretical tools are used to evaluate the temporal evolution of the catalysts. Several mechanisms have been proposed to determine the instability of Pt nanoparticles (and alloys) in low-temperature fuel cells [14, 15]. The various proposed mechanisms are depicted in Fig. 1: (a) and (b) include the formation of ionic species that are then reduced and

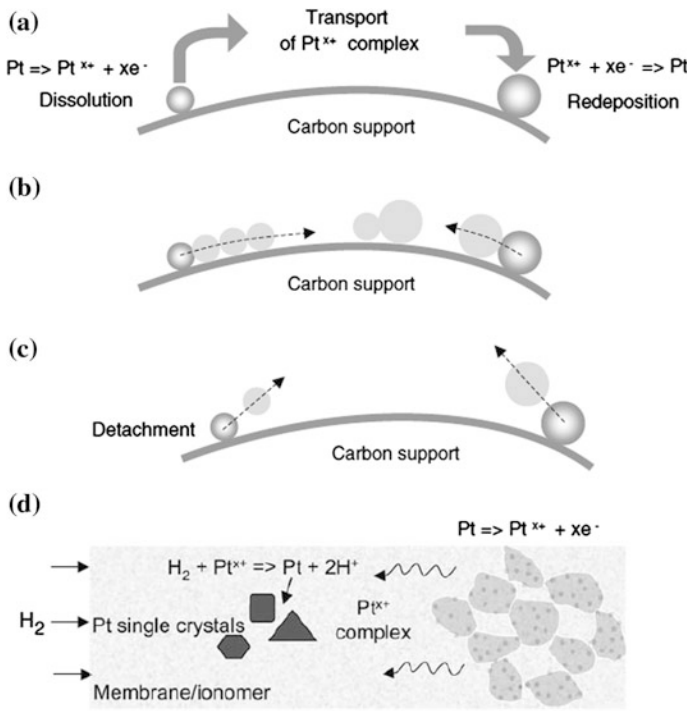

Fig. 1 Main mechanisms for Pt degradation in PEMFC environment. Reprinted with permission from Ref. [15]. **a** Growth via modified ostwald ripening. **b** Coalescence via crystal migration. **c** Detachment from carbon support. **d** Dissolution and precipitation in the ion conductor.

deposited in a larger nanoparticle, or they are reduced by the anodic hydrogen crossover in the membrane. The (b) and (c) mechanisms depend on the mobility of the nanoparticle which is directly related to the substrate–nanoparticle interaction, and to the substrate corrosion. The dissolution of metallic species is modified by the presence of an alloyed element that is more likely to be oxidized than platinum, but also is possible that the alloyed element provokes that the Pt in the surface changes its thermodynamic and kinetic tendency to be detached from the surface. In our research group, we have taken several routes to analyze the stability of metallic nanoparticles in PEFC environments. (1) Using the DFT approach, we investigate the substrate–nanoparticle interaction and its connection with reactivity [16, 17]; (2) Using kinetic Monte Carlo (KMC) techniques, we describe the main processes that are likely to occur in the electrochemical environment such as dissolution and diffusion of the alloy components, reaching simulation times in the order of days; in comparison with simulations of nanoseconds (CMD) or a few picoseconds (AIMD); (3) In a possible structure obtained by the KMC method, we use DFT to analyze the effect that the oxygen atoms in the subsurface have on the adsorbed atoms on the surface. In the two following sections, these approaches are addressed in more detail.

2 Time Evolution by Molecular Dynamics and DFT Simulations

Because of the strong coupling between different physicochemical phenomena, interpretation of the experimental observations is difficult, and analysis through mathematical modeling becomes crucial in order to establish microstructure-performance relationships, elucidate MEA degradation and failure mechanism, and, in the end, help to improve both PEFC electrochemical performance and durability [18]. Different mathematical methods are available to study specific time scales and properties of the system, i.e., the mathematical model includes the description of specific particles and processes occurring. Classical molecular dynamics (CMD) methods use the laws of classical physics to predict the structures and properties of molecules and molecular assemblies. Using this method, we have been able to study the oxidation of Pt(111) and PtCo alloys, using a canonical ensemble NVT (constant number of particles, volume, and temperature), at different oxygen coverage values using Lennard–Jones potentials for the Pt–Pt and Co–Co interactions with parameters fitted to Sutton–Chen potential energy. By assigning negative charges to adsorbed oxygen and positive charges to the Pt atoms in the two topmost layers, we simulated the environment found in a PEFC catalytic system at different electrochemical conditions. The atomic charges used for the simulation were directly obtained by DFT simulations (Bader Charges after optimization). After 900 ps, it was found that oxygen and water produce changes in the structure and local composition of the near-surface layers which may affect the activity and stability of the catalyst. Such changes are strongly dependent

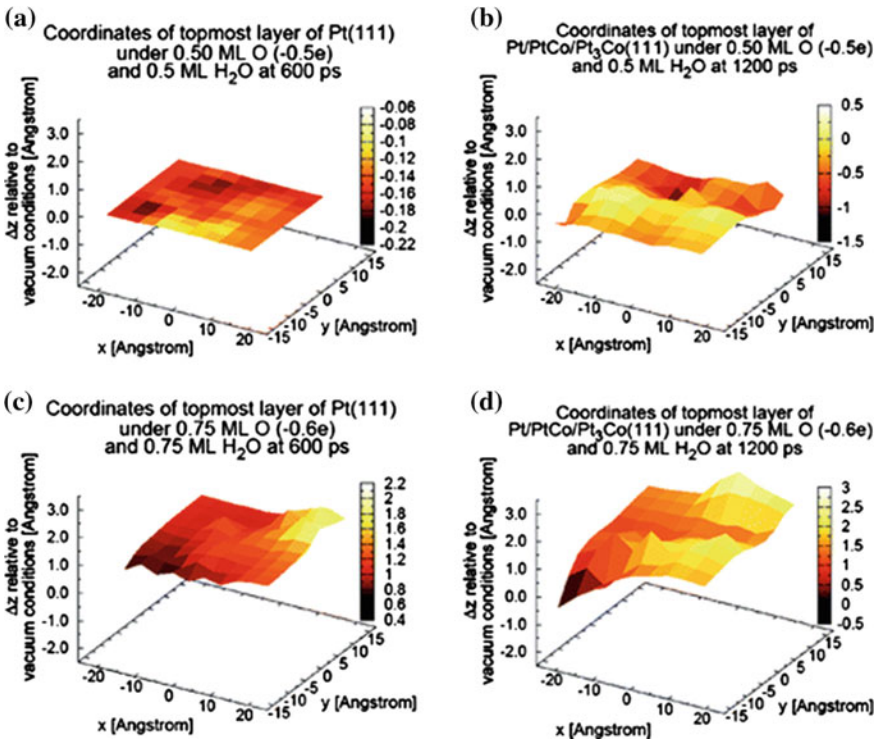

Fig. 2 Molecular dynamics snapshots of the Pt (**a** and **c**) and Pt/PtCo/$PtCo_3$ (**b** and **d**) under different oxygen coverage conditions and electric charge in oxygen. Adapted from Ref. [19]. Reproduced by permission of the PCCP Owner Societies

on the amount of adsorbed oxygen which enhances the segregation of cobalt to the topmost layer. In Fig. 2 (modified from reference [19]), it is possible to observe differences in the topmost layer in a fcc Pt(111) and Pt/PtCo/Pt_3Co at the same conditions of charge and oxygen coverage. It is observed that the separation of the topmost layer from the surface is higher in the alloyed PtCo system than in Pt. In the pure Pt system, the simulation leads to an almost planar structure (Fig. 2a) in comparison to the Pt/PtCo/Pt_3Co system where buckling of atoms is found and is enhanced by augmenting the oxygen coverage. These simulations also were able to confirm the experimental results of oxygen in the subsurface layers [20, 21] and the presence of more bonds Co–O than Pt–O; at oxygen coverage of 0.5 and 0.6 ML, most of the oxygen atoms remain adsorbed on the surface and Co–O bond is only twice more frequent than Pt–O bond. However, for 0.85 of oxygen coverage most of the oxygen atoms are absorbed deeply into the subsurface and the Co–O bonds are three times more frequent than Pt–O bonds.

The absorption of oxygen into the subsurface in pure metals and alloys has been identified as one of the first stages of the catalyst corrosion [22]. In a series of studies using electronic structure methods, analysis of the thermodynamic and

kinetic characteristics of oxygen adsorption and absorption were reported [23–25]. A mechanism for oxygen absorption was found where O migrates from fcc to hcp sites with an energy barrier of 0.63 eV. The transition state geometry is with O in bridge position; then O diffuses into subsurface fcc site with a barrier energy of 2.22 eV and a reverse barrier of 0.7 eV (Fig. 3a). The reverse barrier changes as a function of coverage from 0.7 eV for 0.25 ML to almost zero for 0.11 ML, indicating that subsurface absorption is allowed by higher surface oxygen coverage. It was also reported that the absorption barriers in Pt-alloys are different than those found in pure platinum. For example, the absorption barrier in PtIr is the highest, almost 1 eV higher than in Pt, but in the PtCo alloy, the barrier is only a half of that in pure Pt (Fig. 3b). According to this study, a series of alloys were proposed with Ir as a third alloying component with the highest barriers for oxygen absorption, being an accomplished example of computational design of materials providing guidelines in order to enhance the stability [25].

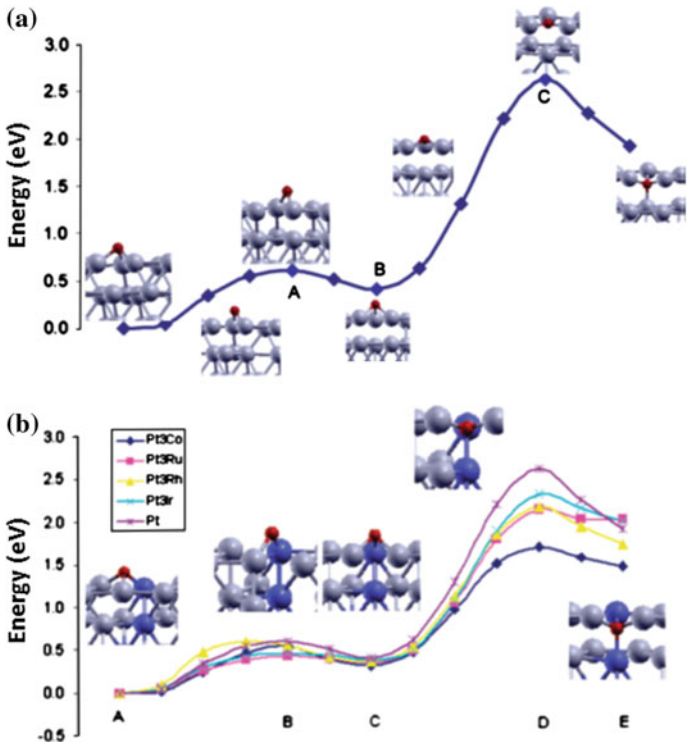

Fig. 3 Energetic barriers for the absorption of oxygen in **a** pure Pt fcc and **b** several PtM alloys where M is a transition metal, adapted from [23–25] (Pt barriers are the same in **a** and **b**). Reprinted with permission from J. Phys. Chem. C., 2007, 111, 9877-9883. Copyright 2007 American Chemical Society; J. Phys. Chem. C, 2007, 111, 17,388-17,396. Copyright 2007 American Chemical Society; J. Phys. Chem. C, 2008, 112, 5057-5065. Copyright 2008 American Chemical Society

3 Time Evolution of PtM Alloys by KMC Methods

Monte Carlo refers to a broad class of algorithms that solve numerical problems through the use of random numbers [26]. A specific coarse-grained Monte Carlo method is that intended for systems evolving dynamically from state to state referred as KMC and widely used for surface reactions, electrochemical systems, and growth processes [27–31]. The dynamical evolution of a system can be studied by molecular dynamics in which one propagates the classical equations of motion forward in time. To do so, one requires suitable interatomic and intermolecular potentials and a set of boundary conditions. The behavior of the system emerges naturally, requiring no intuition or additional input from the user; therefore, the accuracy of the result depends on the parameterization of the atomic forces. A serious limitation is that accurate integration requires time steps short enough to resolve the atomic vibrations. Consequently, the total simulation time in general is limited to much less than one microsecond, usually in the order of tens of nanoseconds. However, the KMC method exploits the fact that the system evolves through diffusive jumps from one state to another, rather than following the vibrational trajectory; consequently, KMC can reach vastly longer scales [32]. Assuming that we know what the possible microscopic events are, we can use transition state theory (TST) to compute the rate constant for each event. Thus, using high-quality TST rates for all possible events, KMC simulations can, in principle, be made as representative of the real process as the results from MD simulations.

Recently, we have reported a KMC algorithm that is able to reproduce the experimental dealloying of Pt-based nanoparticles typically used as oxygen reduction reaction catalyst; the details of the simulation can be found in the original publication [33]. Here, we present a brief introduction to the parameters and reactions used in the original paper. A 3D nanoparticle with metallic structure and lattice parameters optimized using DFT simulations for pure metals and alloys surrounded by a layer of electrolyte is used as starting point. Then each species occupying a site may participate in two reactions: diffusion and dissolution, both described by the Arrhenius equation. The activation energy for the Arrhenius equation includes a bonding energy that depends on (1) the coordination of the atoms and the bonding energy, which was calculated by DFT simulations, and (2) the electric potential of the system by a modification of the Butler–Volmer equation [33] taking into account the transfer factor (having a value of 0.5 for dissolution and 0 for diffusion) and the standard potential for the dissolution of the different metallic atoms. The bonding parameters between Pt and electrolyte were tuned through KMC simulations using the surface diffusion coefficient obtained from experiments and are kept independent of potential.

Using the KMC algorithm, it was possible to study the synthesis of hollow nanoparticles resulting from removal of the alloy core through dealloying using the Kinkerdall effect [34], and the synthesis of porous nanoparticles by selective dealloying of the less noble component. The importance of hollow and porous

nanoparticles resides on their specific area; the specific mass activity is twice higher for the hollow nanoparticles in comparison to the single core–shell structures. For the formation of hollow nanoparticles in a range of particle diameters between 5 and 8 nm, it was found that an applied potential of 12 V is necessary to enhance the diffusion of core species. This is because the core atoms are strongly bonded to their neighbors and these atoms must follow a high-energy path by exchanging positions directly with other metal atoms. In order to have a lower diffusion barrier, the presence of vacancies creates a low-resistance path facilitating the migration of the non-noble metal atoms to the surface where they dissolve. Figure 4 illustrates the required applied voltage for the formation of porous and hollow nanoparticles, which has been discussed previously for nanoparticles with diameter smaller than 15 nm [35]. It is possible to observe ranges of potential in which the structure of the nanoparticle changes drastically, lower potentials lead to core–shell structures, intermediate values to porous, and very high potentials to hollow nanoparticles.

The size of the nanoparticles normally used in fuel cells is $\sim$5 nm. For this reason, we next are interested in the evolution of nanoparticles of this size and potential ranges common to fuel cell conditions 0–1.2 V and with the presence of oxygen. The nature and concentration of species present on the surface of the nanoparticles are functions of the applied potential. Many species can be interacting such as OH, O, O_2, H_2O, and H_2O_2 in different concentrations and their influence can greatly affect the evolution of the nanoparticle. However, inclusion of all these factors makes the simulation much more complex. Thus, at this stage we focus on the influence of oxygen at two potentials 0.9 V with 20 % of oxygen on the surface and 1.2 V with 80 % of oxygen on the surface and 20 % of oxygen in the subsurface [36, 37].

A 5-nm-diameter nanoparticle $Ni_{0.75}Pt_{0.25}$ initially with a random configuration was analyzed by the KMC algorithm. The initial configuration and those after 10^5 and 10^6 s are depicted in Fig. 5. The applied potential is 0.9 V NHE (Normal hydrogen electrode) and oxygen is allowed to interact with the surface forming a

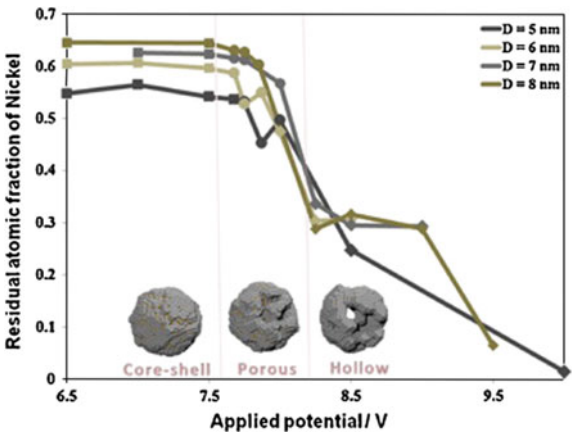

Fig. 4 Structures formed in the Pt–Ni alloy according to the applied potential. Adapted from Ref. [33]

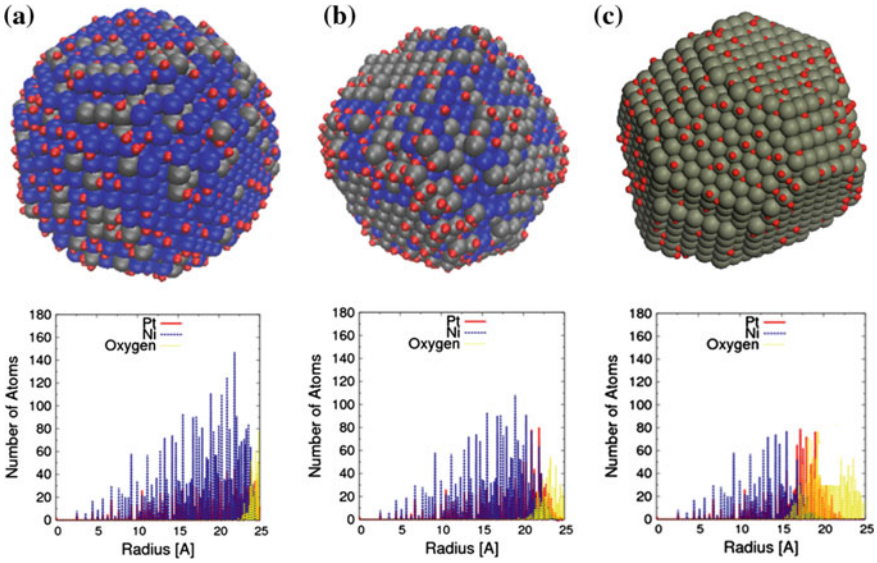

Fig. 5 Evolution of the random alloy as function of time at 0.9 V and 20 % of oxygen coverage. *Top* snapshots (*Blue*, *gray*, and *red spheres* are Ni, Pt, and oxygen, respectively). *Bottom* radial atomic distribution. **a** Initial random configuration, **b** 10^5 s, and **c** 10^6 s (Color figure online)

constant coverage on fcc sites. We emphasize that this alloy has a high Ni percentage at a low potential, in comparison to the potential used for the formation of hollow nanoparticles. The initial random configuration snapshot (Fig. 5a) shows a high concentration of Ni atoms on the surface. After 10^5 s, many Ni atoms dissolve and Pt atoms tend to occupy surface positions, after 10^6 s all the atoms in the surface are Pt and after having reached this configuration, only slight changes are observed. As a consequence of the dissolution of Ni atoms, the nanoparticle gets smaller, the initial radius was 2.5 nm, and at the end of the simulation the nanoparticle has a 2.2-nm radius. These results are in agreement with the previously reported conclusions that at potentials below 7 V the nanoparticle acquires a core–shell configuration. However, in this case the potential is very low and after $\sim$24 h the final configuration shows a total rearrangement of the structure with all the Pt atoms covering the nanoparticle.

The main reason to have a Pt shell with a Pt/Ni core is the dissolution of Ni atoms, rather than diffusion of Pt atoms to the surface. The $Ni_{0.75}Pt_{0.25}$ nanoparticle experiences dissolution of 10 % of the Ni atoms at the very beginning of the simulation and continues all over until the Pt shell is formed. On the other hand, the fraction of Pt atoms that are being dissolved seems to be almost constant (Fig. 6). In order to analyze the influence of different proportions of the alloy constituents, we simulated the $Ni_{0.05}Pt_{0.95}$ and $Ni_{0.25}Pt_{0.75}$ alloys at the same conditions. Figure 6 illustrates that the alloy with 25 % of Ni has almost the same behavior than that with 5 % Ni at short time periods but it reaches faster a constant Ni composition.

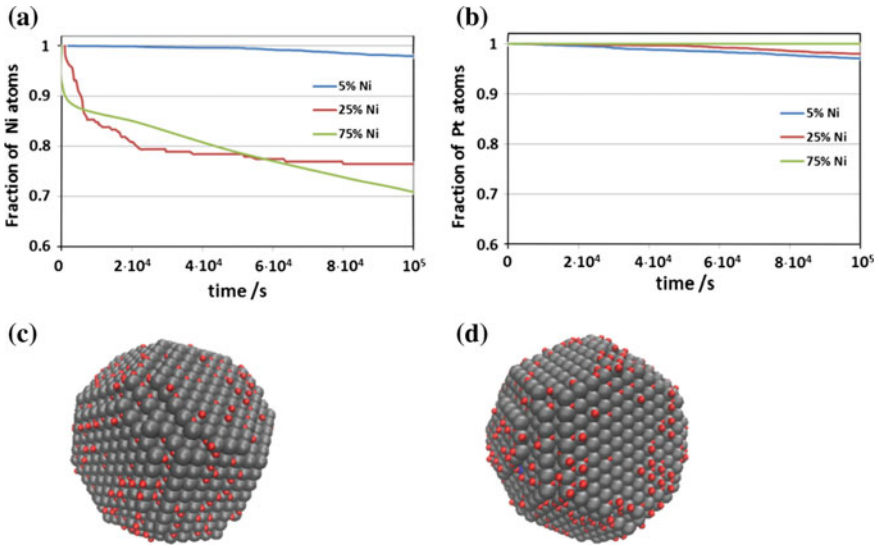

Fig. 6 Fraction of the atoms **a** Ni and **b** Pt as function of time in nanoparticles with different compositions. Snapshots of the final configuration (10^5 s) of the alloys with **c** 25 % Ni and **d** 5 % Ni

The alloy with 5 % loses only a few percent of surface Ni atoms, and then it acquires a more stable configuration that contains a full monolayer of Pt atoms on the surface. The same occurs with the alloy with 25 % Ni. The final configurations for the alloys with 25 and 5 % of Ni are depicted in Fig. 6c and d, respectively; these configurations are attained at 10^5 s in comparison with the alloy with 75 % Ni that requires 10^6 s to achieve the same configuration.

Next, we are interested in the evolution of the same nanoparticle as a function of time at different potentials. The applied potential affects the systems in many ways; it could provide a driving force for the electrochemical dissolution of one of the alloy components or both. It also affects the velocity at which the surface reactions occur (oxygen reduction on the cathode and hydrogen oxidation on the anode of a fuel cell), so it is directly related to the concentration of the surface species. It has been found by both theoretical and experimental techniques that the concentrations of oxygen on the surface and in the subsurface are functions of the potential; therefore, simulations of the nanoparticle at different potentials should include the correct representation of the oxygen concentration. We chose two potentials: (1) 0.9 V at which there is no subsurface oxygen and the concentration of oxygen is 22 % on the hollow fcc sites and (2) 1.2 V at which the concentration of oxygen on the surface is 90 % and the subsurface concentration is 34 %. The adsorption only was allowed on hollow fcc sites on the surface and absorption was allowed in octahedral sites of the subsurface. Figure 7 depicts the time evolution of a nanoparticle with the same diameter (5 nm) at different initial Pt:Ni ratios and at different electrochemical potentials.

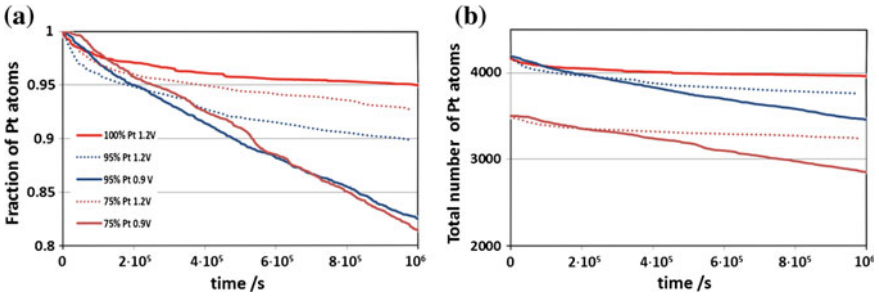

Fig. 7 Time evolution of the platinum atoms in a 5-nm alloy Pt–Ni with the percentage of Pt and potential applied indicated in the legend. **a** Fraction of Pt atoms (with respect to the initial number of Pt atoms) in the nanoparticle, and **b** total number of Pt atoms in the nanoparticle

The nanoparticle composed of 100 % of Pt at 1.2 V presents the lowest dissolution of Pt atoms. At the very beginning of the simulation (0–1 × 10^5 s), the nanoparticles with 75 and 95 % of platinum at 0.9 V show lesser dissolution of Pt atoms, which is related to the preferential dissolution of the Ni atoms. After this time, the pure platinum nanoparticle attains a stable configuration and the number and fraction of Pt atoms is kept almost constant, even at times as higher as 1 × 10^8 s; the nanoparticle fraction of atoms does not change less than 8 %. The total number of atoms and the fraction of atoms as functions of potential follow two different trends. At times lower than 2 × 10^5 s, the nanoparticles at 0.9 V independently of their composition lose a smaller amount of Pt atoms, which is directly related to a higher driving force for dissolution of Ni atoms and consequently higher dissolution. However, after 2 × 10^5 s the system follows the opposite trend, with nanoparticles under a lower potential showing a higher dissolution of Pt atoms. This effect occurs despite of the lower applied potential and that at 1 × 10^5 s at 0.9 V (Fig. 6c, d) the nanoparticle surfaces are composed practically only by Pt atoms. Therefore, at 0.9 V the dissolution of Pt is enhanced by the presence of Ni in the second layer. However, at 1.2 V the higher oxygen concentration allows the formation of an oxide layer that inhibits the dissolution of Pt atoms, but the alloyed nanoparticle presents higher dissolution of Pt atoms than the nanoparticle composed of 100 % of platinum. In general, the dissolution of Pt atoms is enhanced by the presence of an alloying component (Fig. 8).

The fraction of dissolved Ni atoms is higher in comparison to the Pt atoms; at the same elapsed time, the dissolution of Ni atoms reaches values as high as 50 % of the total number of atoms. At the very beginning of the simulation, i.e., when the nanoparticle is allowed to interact with the electrochemical media, more than the 20 % of the Ni is dissolved at 0.9 V; when the nanoparticle is at 1.2 V, only the 10 % of the atoms are lost. The same scenario is observed at higher potentials: the oxygen atoms form an oxide layer that prevents the dissolution of the Ni atoms. As can be observed in Fig. 9, the high O concentration is responsible for the formation of an oxide layer that avoids the detachment of both Pt and Ni atoms.

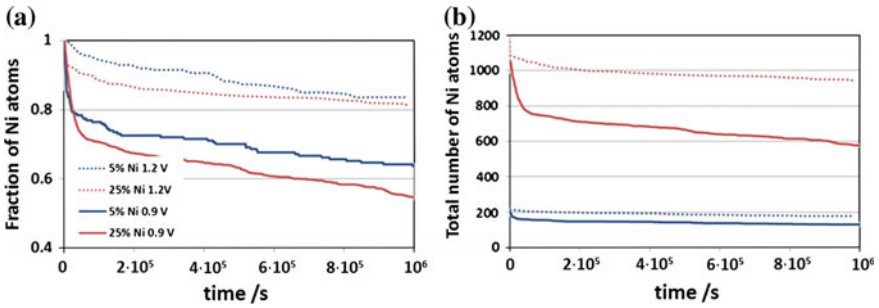

Fig. 8 Time evolution of Ni atoms on the PtNi nanoparticles with the composition and at the potentials indicated in the legend. **a** Fraction of Ni atoms (with respect to the initial number of Ni atoms) as a function of time and **b** total number of Ni atoms as a function of time

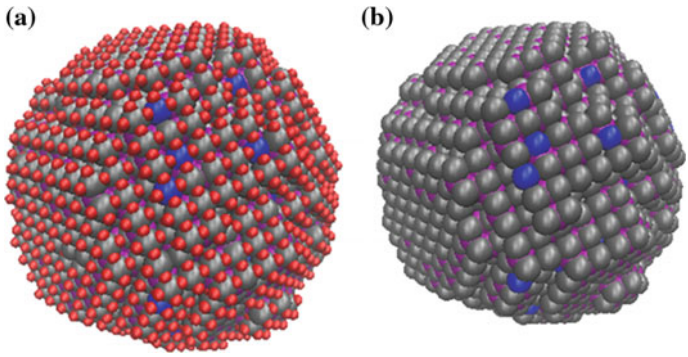

Fig. 9 Snapshot of a $Pt_{0.95}Ni_{0.05}$ at 1.2 V after 1×10^6 s of KMC simulation. *Gray*, *blue*, *red*, and *purple* spheres represent platinum, nickel, oxygen on the surface, and oxygen in the subsurface, respectively. **a** Structure showing oxygen on the surface, **b** surface oxygen is not shown to better visualize the surface and subsurface composition (Color figure online)

Note that more Ni atoms are observed on the surface in contrast with Fig. 6, where most of the atoms on the surface are platinum.

The results here obtained have important implications: (1) The formation of a metallic alloy in order to enhance the ORR kinetics causes enhanced degradation owed to the dissolution of the less noble alloyed metal but also to the enhanced dissolution of Pt in comparison to the pure nanoparticle. (2) The formation of an oxide layer at 1.2 V avoids the degradation of the nanoparticle; however, the usual range of operation of this nanoparticles is 0.6–1.0 V which imply that dissolution of the components in this range is expected. (3) The subsurface concentration of oxygen has been kept constant, and it is essential for improved results to investigate the mobility and effect that these atoms may have on the detachment of Pt and alloyed metals. And (5) Of special importance is the analysis of dynamic potential, i.e., what would be the effect of potential steps or potential sweep on the stability of the nanoparticles. This will be reported elsewhere.

4 Degradation of PtCo Skin

In the previous section, the position and charge of oxygen in the subsurface was kept constant; however, those changes should be analyzed along with the effect on the structure of the surface. Thus, in this section the evolution of a Pt/PtCo skin system is analyzed using DFT after the absorption of oxygen in the subsurface. The system used for the simulations consists of a 2 × 2 fcc slab containing five layers separated by a 12 Å vacuum. The three first layers were allowed to relax, while the last two are kept fixed. The first layer has only Pt atoms, the second only Co atoms, and from the third to fifth a 1:1 composition. This system is the one previously reported by our group as the most stable obtained by DFT simulations, as well as confirmed by the KMC simulated experiments [38]. We have analyzed the influence of the O coverage factor on the stability of the PtCo system. We probed first the adsorption energy of oxygen either in the surface or in the subsurface for the formation of a 0.25 ML. In previous studies, it was found that the preferential sites for oxygen adsorption are the three-coordinated ones over atop and bridge sites [39–41]. In this work, we use the fcc and hcp sites for oxygen adsorption on the surface and the sub-fcc, sub-hcp, and sub-tet, all of them are depicted in Fig. 10. In the hcp site, the oxygen is above a Co atom in the second layer; in the fcc site, on the other hand, the oxygen is in line with a Pt atom in the third layer. The hcp-sub and fcc-sub sites are the counterparts of the hcp and fcc sites on the surface, the hcp-sub site is in a tetrahedral hollow, and the fcc-sub site is in an octahedral hollow. The tet-sub site is also in a tetrahedral hollow but in this case the interaction is with three cobalt atoms in the second layer and one platinum atom in the first

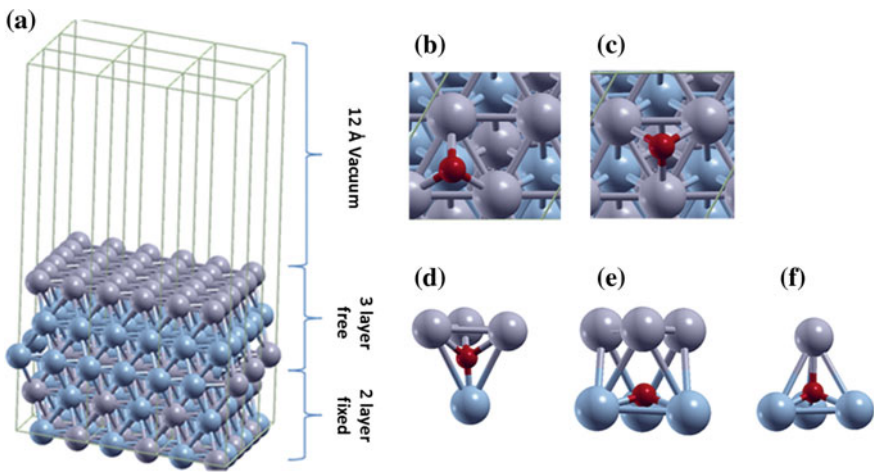

Fig. 10 **a** Slab model. Sites for oxygen adsorption: **b** hcp, **c** fcc; and for oxygen absorption in the subsurface: **d** hcp-sub, **e** tet-sub, and **f** fcc-sub. *Blue*, *gray*, and *red* spheres represent Co, Pt, and O atoms, respectively (Color figure online)

Table 1 Energetic and some geometrical values of O adsorption on the surface and absorption in the subsurface sites

		hcp	fcc	hcp-sub	tet-sub	fcc-sub
E_{ads}/eV	RPBE	−2.38	−2.57	+0.12	−1.99	−1.156
	PBE [43]	−2.94	−3.15			
	Pd@Co (PW91) [44]	−2.5				
Distance/Å	Pt–O	2.12	2.10	1.98	2.11	2.68
	Pt–O [43]	2.1	2.1			
	Co–O			1.80	1.86	1.82

layer, while in the hcp the interaction is with one cobalt atom in the second layer and three Pt atoms in the first layer. The adsorption energy is reported in Table 1, compared with results from other publications.

The adsorption energy calculated for the formation of 0.25 ML with the RPBE [42] exchange correlation functional is weaker in comparison with the PBE functional; however, the same trends are obtained with both exchange correlation functionals. The O adsorption energy in the surface is higher than the absorption in the subsurface, and interestingly the absorption in the hcp-sub site presents positive adsorption energy. The most stable site for adsorption on the surface is the fcc with very similar values for the hcp site, and the most stable site for the absorption in the subsurface is the tet-sub site. In any of the subsurface sites in the subsurface, the O atom has a tendency to stay closer to the Co than to the Pt atoms.

It is interesting to analyze what are the physical consequences of the oxygen adsorption on each interaction site. We focus on the vertical displacement of the surface atoms (buckling) and the charge of the atoms. The vertical displacement is defined as the difference in the position of the atom in the vertical direction before and after the interaction with oxygen and is directly related to the capacity of the atoms in the surface to remain bonded to the surface (negative or null displacement) or tendency to escape from the surface (positive displacement). The charge of the metallic atom is also related to the oxidation state of the atom, and a positive charge indicates that the atom is in a more oxidized state.

O adsorption, either in fcc or hcp sites, promotes a slightly positive buckling of Pt atoms; however, in comparison to the buckling induced by O in the subsurface it is almost negligible. Previously, we have stated that the O atoms in the subsurface have the tendency to occupy positions closer to Co atoms, and in this sense we expected that it would have more influence on Co than on Pt atoms. In the hcp-sub site, we found that all the Pt atoms suffered positive buckling, especially the atoms directly interacting with oxygen; on the other hand, the Co atom directly interacting with oxygen suffers negative displacements, while the other Co atoms present slightly positive buckling. Similar behavior is observed in the fcc-sub site where all the Pt atoms experienced positive displacement in the same magnitude than in the hcp-sub site. The Co atoms directly interacting with O do not change their positions but the one that is not directly interacting suffers a positive displacement of the

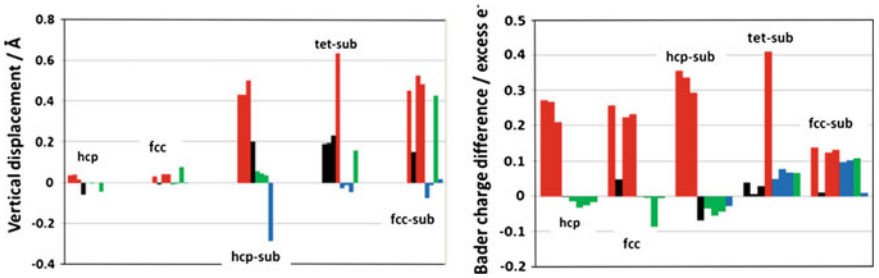

Fig. 11 Vertical displacement and Bader charge of surface and subsurface atoms. *Red bars* represent Pt atoms directly interacting with oxygen; *black bars* represent Pt atoms not in direct contact with oxygen. *Blue bars* represent Co atoms directly interacting with oxygen; *green bars* represent Co atoms not directly in contact with oxygen (Color figure online)

same magnitude than those of the Pt atoms. Interacting in the tet-sub site, the Pt atom directly above the oxygen in the subsurface presents the highest vertical positive displacement, but also the other Pt atoms not directly interacting with oxygen, whereas the Co atom that is not in contact with oxygen suffers a positive vertical displacement (Fig. 11).

In the surface of the clean PtCo skin, the Co atoms have positive charge (about +0.3 e/atom), while the Pt atoms in the deepest layers have negative values (−0.4 e/atom); however, the Pt atoms at the surface have a lesser negative value around −0.22 e/atom. After O adsorption if the change on the charge of platinum atoms is greater than 0.22, the atom changes to a slightly oxidized state. Most of the different O positions either in the surface or subsurface lead to at least one Pt atom in an oxidized state. Although expected, it is worth to mention that when O is on the surface the Pt atoms directly interact with it, and become oxidized, while the no interacting atom remains with partial negative charge. In the hcp-sub site, all the Pt atoms have a more drastic change in charge becoming more oxidized, while the Co and Pt atoms not in contact with oxygen gain electronic charge. In the tet-sub site, only the Pt atom directly interacting with oxygen lose electronic charge; however, all the other Pt or Co atoms also lose charge but do not acquire partial positive charge. Finally, in the fcc-sub site Pt and Co atoms directly interacting with oxygen lose electron density; this site is where the Co atoms lose the highest charge density, which already was positive. Summarizing, the interaction with oxygen leads to a positive charge in the Pt atoms, and the Co atoms are also affected but in a lesser degree even if the oxygen is in the subsurface and closer to the Co than to the Pt atoms; however, the charge of Co atoms was already even more positive than those of any Pt atom. Energetically, the least favorable site on the subsurface is the hcp-sub site in which the Pt atoms are highly oxidized and the Co atoms gain charge, and the most stable is the tet-sub site with one Pt atom bearing high positive charge and a large positive vertical displacement.

After considering the consequences of the O adsorption on the surface and absorption in the subsurface, we want to analyze what is the influence of O in the

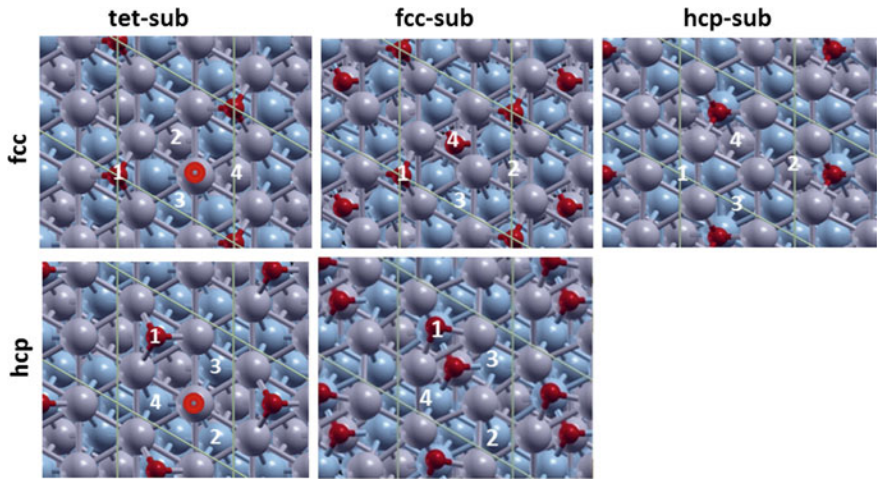

Fig. 12 Sites for adsorption of the four atoms on the surface, the column labels indicate the O site in the subsurface, and the row labels the position for O on the surface. The numbers indicate the order, which were allowed to adsorb; *1* = 0.25 ML, *2* = 0.5 ML, *3* = 0.75 ML, *4* = 1 ML

subsurface in both the adsorption energy of oxygen on the surface from 0.25 to 1 ML and the changes in vertical displacement and charge of the atoms.

Previous calculations performed by our group have shown that the energetic barrier for the absorption of oxygen is lower in the case of PtCo alloys (1.39 eV) in comparison to pure platinum (2.22); but also the energetic barrier for the reverse process is lower in PtCo (0.23 eV) than in Pt (0.7 eV) [25]. In order to allow the absorbed oxygen to desorb, the positions of the oxygen atoms on the surface (Fig. 12) were kept the farthest away from the absorbed oxygen atom during the process of completing the full coverage. In none of our simulations, the absorbed oxygen was desorbed from the subsurface, but the oxygen atom on the position with the lowest energy (hcp-sub) moved to the highest one (tet-sub), as in the case of the absorption in the hcp-sub site with adsorption in the hcp site. In this site, for all coverage values the oxygen in the subsurface changed to the tet-sub site. In all other combinations, the absorbed oxygen does not move from its original position as shown in Fig. 13, which illustrates the structural evolution of the slab as a function of the coverage, for every location of O in the subsurface and O adsorbed on the surface on the fcc sites. For comparison, we show the structural evolution of the system without oxygen in the subsurface as the oxygen coverage on the surface is changed.

The evolution of the system as a function of the surface oxygen coverage without oxygen in the subsurface is relatively simple. There are no major changes, and only at 0.75 ML the structure shows buckling but not as extreme as when the oxygen has been absorbed. For the system with oxygen located in the tet-sub position of the subsurface, the Pt atom above O is observed to protrude slightly above the surface. The vertical displacement is enhanced as the coverage augments,

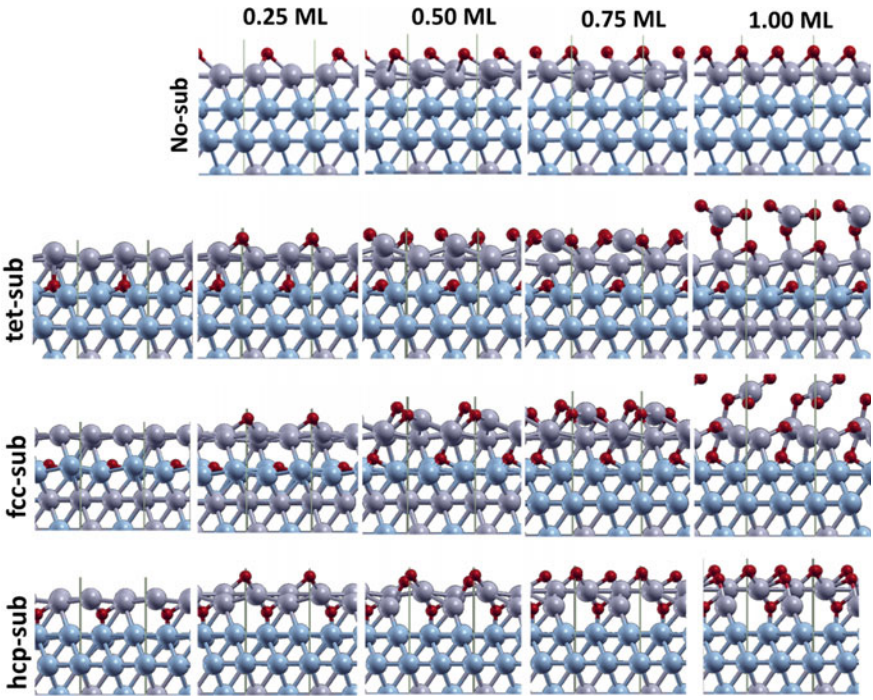

Fig. 13 Snapshots of the optimized structures at different oxygen coverage values with oxygen in the subsurface (2nd, 3rd, and 4th row) and without oxygen on the subsurface (1st row). *Gray*, *blue*, and *red spheres* represent platinum, cobalt, and oxygen atoms, respectively (Color figure online)

not for all the atoms but only for that atom originally located above the O; even if the Pt–O has been broken and the oxygen remains close to the Co atoms, the Pt atom continuously moves away from the surface. The final vertical displacement of the Pt atom with O on the surface at the fcc positions is 2.77 Å and with oxygen in hcp positions is 3.19 Å. All other atoms including Co and O remained in their same sites. Similar behavior is observed when O is in the fcc-sub site; at 1 ML coverage, one of the Pt atoms is bonded to the absorbed oxygen and another is detached from the surface, and the final vertical displacement of the Pt atom is 3.21 Å. The scenario changes when O is in the hcp-sub site. In that case, the O atom in the subsurface keeps linked to three Pt atoms. Surface detachment is observed even for very low O coverage factors but for all atoms in the same magnitude and no detachment is observed at full coverage; the three atoms moved from their original position but only 0.8 Å which is a minimum displacement in comparison to those induced by O in the fcc-sub and tet-sub sites.

In the charge analysis reported above, it was found that the Pt atom located directly above of the subsurface tet-sub oxygen has a net positive Bader charge, while the other Pt atoms in the first layer (atoms 1–4) retain their negative charge (water blue symbols in Fig. 14 left), and the Pt atoms in the third, fourth, and fifth

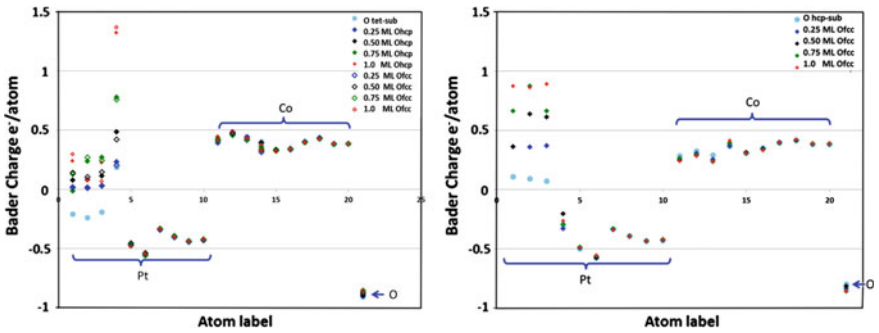

Fig. 14 Bader charges of all slab atoms as functions of the O coverage on the surface. *Left* O in the subsurface in tet-sub site; *Right* O in the subsurface in hcp-sub position. Atom label: 1–10 Pt; 11–20 is the Co and 21 is the O in the subsurface. Symbols represent Bader charges for every coverage having O atoms on the surface in fcc sites (*closed symbols*) and hcp sites (*open symbols*)

layers (atoms 6–10) retain their negative charge. The Co atoms, on the other hand, have a positive charge; the most positive corresponds to those in the second layer (atoms 11–14). All the Pt atoms in the first layer (1–4) increase their charge as the coverage augments; however, the Pt atom directly above the subsurface O is the one that increases its charge more rapidly, despite the fact that the O atoms added to augment the O coverage are placed the farthest away from this atom. The highest value reached is close to +1.5 and this atom becomes separated from the surface by more than 3 Å, clearly suggesting that this atom is ready to dissolve in the electrolyte or move to sites where it is able to receive electrons. The Co atoms in the second layer interestingly do not change their charge value neither their positions. During absorption of the O atom in the subsurface, the Co atoms do not change their charge value; therefore, in all the study the Co atoms are slightly affected by the subsurface atom and by the changes in the coverage.

The changes in the system charges with hcp-sub O are different. The three Pt atoms bonded to the subsurface O augment their charge value roughly in the same magnitude as the coverage increases; the maximum charge value reached in this site is lesser than +1 for all the atoms. The Co atoms in the second layer have lesser positive charges in comparison to the tet-sub site. In all the systems with subsurface O, the charges and positions of atoms in the second layer and deeper remain unaffected. In the system without subsurface O, the situation is totally different: the maximum charge reached by the Pt atoms in the fully oxygenated surface is +0.38 and that of the Co atoms is +0.3. We then can state that once O is in the subsurface despite the low barrier for desorption, the atom remains in the subsurface, and it eventually will lead to the detachment of the Pt atom directly above it. By keeping lower oxygen coverage, lesser than 0.5 ML, one ensures that the vertical displacement of the atom and its charge attains values similar to the system without subsurface O.

The adsorption energy was calculated as follows:

$$E_{ad} = E_{slab\text{-}O} - (E_{slab} - E_O) \quad (1)$$

where E_{ad} is the adsorption energy, E_{slab} is the energy of the clean system, $E_{slab\text{-}O}$ is the energy of the system with oxygen adsorbed either on the surface or in the subsurface, and E_O is the energy of the free oxygen atom. For subsequent adsorption steps, i.e., to augment the coverage, the reference energy (E_{slab}) is changed by the energy of the slab with a lesser oxygen atom and calculated in the same manner. For example, to calculate the E_{ad} for 0.75 ML, we use $E_{ad0.75ML} = E_{0.75ML} - (E_{0.50ML} - E_O)$. The relative energy is calculated as follows:

$$E_{rel} = E_{slab\text{-}nO} - (E_{slab} - nE_O) \quad (2)$$

where E_{rel} is the energy relative to the clean surface, $E_{slab\text{-}nO}$ is the slab with n oxygen atoms either in the subsurface or on the surface, and nE_0 is n times the energy of the free oxygen.

At zero coverage, the adsorption energy on the surface is stronger than the absorption in the subsurface; however, once O is in the subsurface the relative energy of the system with subsurface O is higher than that of the system without oxygen absorbed. Therefore, there is a thermodynamic driving force for one of the oxygen atoms on the surface to go to the subsurface; however, as previously mentioned the barrier for the atom to move to the subsurface is high at low coverage, and at high coverage the system stabilizes subsurface atomic oxygen from energetic and kinetic point of view [24]. The binding energy of the system with subsurface O is higher when the atom is in the tet-sub site at 0.25 ML, but at 0.5 and 0.75 ML the fcc-sub site has the highest binding energy, and at 1 ML they have the same binding energy; however, both the tet-sub and fcc-sub sites have similar values. The hcp site yields the weakest binding energy and in fact the site easily changes to tet-sub or fcc-sub site. In the full coverage situation, the hcp site without subsurface O yields stronger binding than the hcp-sub site indicating that this system has low probability to subsist changing either from the hcp-sub to fcc-sub site or desorbing the oxygen from the subsurface. The analysis of the total energy of systems with and without subsurface O could lead to misleading conclusions as the number of atoms is different in each system; however, if the relative energy of the system without subsurface O (red lines in Fig. 15) is moved 0.25 ML to the left, the same conclusions are reached: the system with subsurface O is more stable than the one without it.

The adsorption energy has been used as a descriptor of the catalytic activity, and most of the studies for the ORR on metallic surfaces have been tested in a 0.25 ML system [45], including that higher coverage is risky owed that the van der Waals interactions will play a more important role between adjacent molecules. Anyway the different values will give an idea of the changes in catalytic activity. The hcp-sub site is the system with the lowest binding energy. At all coverage situations, the binding energy in this site is the weakest one and possibly this situation

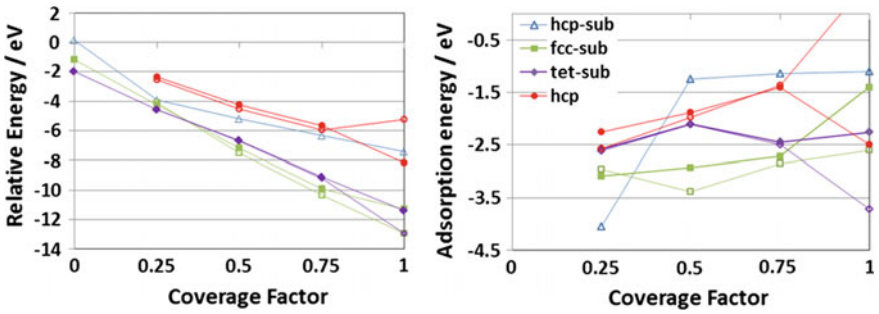

Fig. 15 Energetic values for oxygen adsorption as function of O coverage in fcc sites (*closed symbols*) and hcp sites (*open symbols*) with subsurface O in the positions indicated in the legend (legend is the same for both graphs) and without subsurface O (*red symbols*). Lines are drawn as guide for the eye. (Equations are explained in the main text). The legend indicates the oxygen in the subsurface. Two lines are drawn with the same color, one for the adsorption of oxygen in the fcc sites (*closed symbols*) and in the hcp sites (*open symbols*) (Color figure online)

never takes place. The binding energy is very similar in the tet-sub site to the situation without subsurface O. The binding energy in the systems without subsurface O tends to diminish as the coverage is increased, as expected due to higher interactions between adjacent molecules. The binding energy even reaches positive values at the full coverage system in the fcc sites. In the hcp site, the behavior is different because the surface O changes from hcp to top or bridge positions. In the systems with subsurface O, as one of the metal atoms moves away from the surface, the interactions between O atoms are weaker and in consequence the adsorption energy maintains the same values.

5 Concluding Remarks

A multi-scale modeling approach shows new insights regarding oxidation effects on alloy surfaces and nanoparticles. Combined DFT–classical MD simulations illustrate the time evolution of the catalyst surface as the oxygen coverage increases. The observed buckling is in agreement with previous DFT results where we investigated the adsorption and absorption of oxygen in alloy surfaces. Kinetic Monte Carlo simulations are used to determine the effect of an alloy on Pt dissolution under an electrochemical potential corresponding to the onset of surface oxidation. It is found that before the surface oxidation starts, first the dissolution of the non-noble metal takes place, and it is followed by the formation of a Pt shell on the surface of the nanoparticle. However, after the onset of surface oxidation, the oxidation film passivates the surface and stops metal dissolution; further research should be done on the effect of this passivating film on the catalytic activity. Finally, DFT calculations are utilized to understand the O-induced degradation of Pt–Co alloys at

various coverage values. When there is no oxygen in the subsurface, structural changes are observed only at high surface coverage (>0.75 ML of O). In contrast, significant structural changes are detected when O is in the subsurface. Although buckling and surface reconstruction are observed for O absorbed in any of the subsurface sites, the most dramatic correspond to O absorbed in tet-sub and hcp-sub sites. The Co atoms in the second layer interestingly do not change their charge value or their positions. During absorption of the O atom in the subsurface, the Co atoms do not change their charge value; therefore, in all the study the Co atoms are slightly affected by the subsurface atom and by the changes in the coverage. It should be interesting to determine the mechanism for the Co atoms to move from the subsurface where they interact strongly with oxygen to the surface for their further dissolution.

References

1. Song CS (2006) Global challenges and strategies for control, conversion and utilization of CO_2 for sustainable development involving energy, catalysis, adsorption and chemical processing. Catal Today 115:2–32
2. Specht M, Staiss F, Bandi A, Weimer T (1998) Comparison of the renewable transportation fuels, liquid hydrogen and methanol, with gasoline-energetic and economic aspects. Int J Hydrogen Energy 23:387–396
3. Stamenkovic V, Schmidt TJ, Ross PN, Markovic NM (2002) Surface composition effects in electrocatalysis: Kinetics of oxygen reduction on well-defined Pt_3Ni and Pt_3Co alloy surfaces. J Phys Chem B 106:11970–11979
4. Xiong LF, Manthiram A (2004) Influence of atomic ordering on the electrocatalytic activity of Pt-Co alloys in alkaline electrolyte and proton exchange membrane fuel cells. J Mater Chem 14:1454–1460
5. Vinayan BP, Nagar R, Rajalakshmi N, Ramaprabhu S (2012) Novel platinum-cobalt alloy nanoparticles dispersed on nitrogen-doped graphene as a cathode electrocatalyst for PEMFC applications. Adv Funct Mater 22:3519–3526
6. Cui C, Gan L, Li H-H, Yu S-H, Heggen M, Strasser P (2012) Octahedral PtNi nanoparticle catalysts: exceptional oxygen reduction activity by tuning the alloy particle surface composition. Nano Lett 12:5885–5889
7. Loukrakpam R, Luo J, He T, Chen Y, Xu Z, Njoki PN, Wanjala BN, Fang B, Mott D, Yin J, Klar J, Powell B, Zhong C-J (2011) Nanoengineered PtCo and PtNi catalysts for oxygen reduction reaction: an assessment of the structural and electrocatalytic properties. J Phys Chem C 115:1682–1694
8. Gasteiger HA, Kocha SS, Sompalli B, Wagner FT (2005) Activity benchmarks and requirements for Pt, Pt-alloy, and non-Pt oxygen reduction catalysts for PEMFCs. Appl Catal B Environ 56:9–35
9. Xie J, Wood DL, Wayne DM, Zawodzinski TA, Atanassov P, Borup RL (2005) Durability of PEFCs at high humidity conditions. J Electrochem Soc 152:A104–A113
10. Ramos-Sanchez G, Solorza-Feria O (2010) Synthesis and characterization of Pd0.5NixSe (0.5-x) electrocatalysts for oxygen reduction reaction in acid media. Int J Hydrogen Energy 35:12105–12110
11. Borup RL, Davey JR, Garzon FH, Wood DL, Inbody MA (2006) PEM fuel cell electrocatalyst durability measurements. J Power Sources 163:76–81

12. Iojoiu C, Guilminot E, Maillard F, Chatenet M, Sanchez JY, Claude E, Rossinot E (2007) Membrane and active layer degradation following PEMFC steady-state operation—II. Influence of Ptz+ on membrane properties. J Electrochem Soc 154:B1115–B1120
13. Dubau L, Durst J, Maillard F, Guetaz L, Chatenet M, Andre J, Rossinot E (2011) Further insights into the durability of Pt3Co/C electrocatalysts: formation of "hollow" Pt nanoparticles induced by the Kirkendall effect. Electrochim Acta 56:10658–10667
14. Ferreira PJ, Ia OGJ, Shao-Horn Y, Morgan D, Makharia R, Kocha S, Gasteiger HA (2005) Instability of Pt/C electrocatalysts in proton-exchange membrane fuel cells. J Electrochem Soc 152:A2256–A2271
15. Shao-Horn Y, Sheng WC, Chen S, Ferreira PJ, Holby EF, Morgan D (2007) Instability of supported platinum nanoparticles in low-temperature fuel cells. Top Catal 46:285–305
16. Ramos-Sanchez G, Balbuena PB (2013) Interactions of platinum clusters with a graphite substrate. Phys Chem Chem Phys 15:11950–11959
17. Ma J, Habrioux A, Morais C, Lewera A, Vogel W, Verde-Gomez Y, Ramos-Sanchez G, Balbuena PB, Alonso-Vante N (2013) Spectroelectrochemical probing of the strong interaction between platinum nanoparticles and graphitic domains of carbon. ACS Catal 3:1940–1950
18. Franco AA, Tembely M (2007) Transient multiscale modeling of aging mechanisms in a PEFC cathode. J Electrochem Soc 154:B712–B723
19. Callejas-Tovar R, Balbuena PB (2011) Molecular dynamics simulations of surface oxide-water interactions on Pt(111) and Pt/PtCo/Pt_3Co(111). Phys Chem Chem Phys 13:20461–20470
20. McMillan N, Lele T, Snively C, Lauterbach J (2005) Subsurface oxygen formation on Pt(100): experiments and modeling. Catal Today 105:244–253
21. Walker AV, Klotzer B, King DA (2000) The formation of subsurface oxygen on Pt{110} (1 × 2) from molecular-beam-generated O-2 (1)Delta(g). J Chem Phys 112:8631–8636
22. Over H, Seitsonen AP (2002) Oxidation of metal surfaces. Science 297:2003–2005
23. Gu Z, Balbuena PB (2007) Absorption of atomic oxygen into subsurfaces of Pt(100) and Pt (111): density functional theory study. J Phys Chem C 111:9877–9883
24. Gu Z, Balbuena PB (2007) Chemical environment effects on the atomic oxygen absorption into Pt(111) subsurfaces. J Phys Chem C 111:17388–17396
25. Gu Z, Balbuena PB (2008) Atomic oxygen absorption into Pt-based alloy subsurfaces. J Phys Chem C 112:5057–5065
26. Allen MP, Tildesley DJ (1990) Computer simulation of liquids. Oxford University Press, Oxford
27. Koper MTM, Jansen APJ, vanSanten RA, Lukkien JJ, Hilbers PAJ (1998) Monte Carlo simulations of a simple model for the electrocatalytic CO oxidation on platinum. J Chem Phys 109:6051–6062
28. Koper MTM, Lukkien JJ, Jansen APJ, Van Santen RA (1999) Lattice gas model for CO electrooxidation on Pt-Ru bimetallic surfaces. J Phys Chem B 103:5522–5529
29. Lukkien J, Segers JPL, Hilbers PAJ, Gelten RJ, Jansen APJ (1998) Efficient Monte Carlo methods for the simulation of catalytic surface reactions. Phys Rev E 58:2598–2610
30. Mainardi DS, Calvo SR, Jansen APJ, Lukkien JJ, Balbuena PB (2003) Dynamic Monte Carlo simulations of O_2 adsorption and reaction on Pt(111). Chem Phys Lett 382:553–560
31. Van Gelten RJ, Jansen APJ, Van Santen RA, Lukkien JJ, Segers JPL, Hilbergs PAJ (1998) Monte Carlo simulations of a surface reaction model showing spatio-temporal pattern formations and oscillations. J Chem Phys 108:5921–5934
32. Voter AF (2007) Introduction To The kinetic Monte Carlo method, vol 235
33. Callejas-Tovar R, Diaz CA, Hoz JMMdI, Balbuena PB (2013) Dealloying of platinum-based alloy catalysts: kinetic Monte Carlo simulations. Electrochim Acta 101:326–333
34. Kirkendall E, Thomassen L, Uethegrove C (1939) Rates of diffusion copper and zinc in alpha brass. Trans Am Inst Mining Metall Eng 133:186–203
35. Erlebacher J, Aziz MJ, Karma A, Dimitrov N, Sieradzki K (2001) Evolution of nanoporosity in dealloying. Nature 410:450–453

36. Holby EF, Greeley J, Morgan D (2012) Thermodynamics and hysteresis of oxide formation and removal on platinum (111) surfaces. J Phys Chem C 116:9942–9946
37. Wakisaka M, Asizawa S, Uchida H, Watanabe M (2010) In situ STM observation of morphological changes of the Pt(111) electrode surface during potential cycling in 10 mM HF solution. Phys Chem Chem Phys 12:4184–4190
38. Hirunsit P, Balbuena PB (2009) Surface atomic distribution and water adsorption on PtCo alloys. Surf Sci 603:911–919
39. Pokhmurskii V, Korniy S, Kopylets V (2011) Computer simulation of binary platinum-cobalt nanoclusters interaction with oxygen. J Cluster Sci 22:449–458
40. Yang ZX, Yu XH, Ma DW (2009) Adsorption and diffusion of oxygen atom on Pt3Ni(111) surface with Pt-skin. Acta Phys Chim Sin 25:2329–2335
41. Leisenberger FP, Koller G, Sock M, Surnev S, Ramsey MG, Netzer FP, Klotzer B, Hayek K (2000) Surface and subsurface oxygen on Pd(111). Surf Sci 445:380–393
42. Hammer B, Hansen LB, Norskov JK (1999) Improved adsorption energetics within density-functional theory using revised Perdew-Burke-Ernzerhof functionals. Phys Rev B 59:7413–7421
43. Hirunsit P, Balbuena PB (2009) Effects of water and electric field on atomic oxygen adsorption on PtCo alloys. Surf Sci 603:3239–3248
44. Tang W, Henkelman G (2009) Charge redistribution in core-shell nanoparticles to promote oxygen reduction. J Chem Phys 130
45. Norskov JK, Rossmeisl J, Logadottir A, Lindqvist L, Kitchin JR, Bligaard T, Jonsson H (2004) Origin of the overpotential for oxygen reduction at a fuel-cell cathode. J Phys Chem B 108:17886–17892

http://www.springer.com/978-1-4471-5676-5

Physical Multiscale Modeling and Numerical Simulation of Electrochemical Devices for Energy Conversion and Storage

From Theory to Engineering to Practice

Franco, A.A.; Doublet, M.L.; Bessler, W.G. (Eds.)

2016, VII, 249 p., Hardcover
ISBN: 978-1-4471-5676-5